Accepted Manuscript

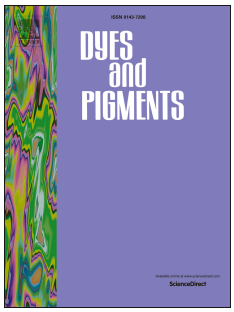

A new series of *N*-substituted tetraphenylethene-based benzimidazoles: Aggregation-induced emission, fast-reversible mechanochromism and blue electroluminescence

Tengfei Zhang, Ran Zhang, Yun Zhao, Zhonghai Ni

PII: S0143-7208(17)31313-X

DOI: 10.1016/j.dyepig.2017.09.018

Reference: DYPI 6242

To appear in: *Dyes and Pigments*

Received Date: 10 June 2017

Revised Date: 6 September 2017

Accepted Date: 8 September 2017

Please cite this article as: Zhang T, Zhang R, Zhao Y, Ni Z, A new series of *N*-substituted tetraphenylethene-based benzimidazoles: Aggregation-induced emission, fast-reversible mechanochromism and blue electroluminescence, *Dyes and Pigments* (2017), doi: 10.1016/j.dyepig.2017.09.018.

A new series of *N*-substituted tetraphenylethene-based benzimidazoles were designed and synthesized. These compounds are blue fluorescence in crystalline state and show fast-reversible mechanochromism. Furthermore, both of non-doped OLED devices fabricated with compounds **3b** and **3c** as emitters are blue emission.

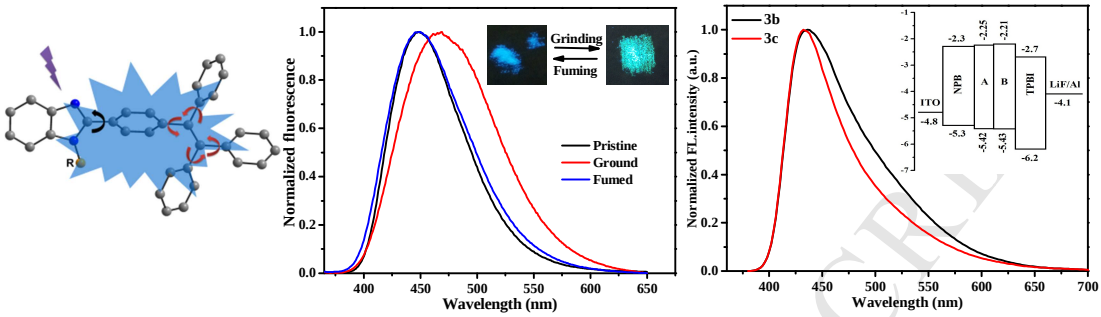

A new series of *N*-substituted tetraphenylethene-based benzimidazoles: aggregation-induced emission, fast-reversible mechanochromism and blue electroluminescence

Tengfei Zhang, Ran Zhang, Yun Zhao, Zhonghai Ni*

School of Chemical Engineering and Technology, China University of Mining and Technology, Xuzhou 221116, Jiangsu Province, P. R. China

Tel: +86-516-83883927

Corresponding author E-mail: nizhonghai@cumt.edu.cn

Abstract

Four new *N*-substituted tetraphenylethene-based benzimidazoles *N*-R-2-(4-(1,2,2-triphenylvinyl)phenyl)-1*H*-benzo[*d*]imidazoles (R = phenyl (**3a**), R = 4-(*tert*-butyl)phenyl (**3b**), R = *n*-butyl (**3c**), R = *n*-hexyl (**3d**)) were synthesized conveniently by cyclization reaction of 4-tetraphenylenthenealdehyde with *N*-substituted *ortho*-nitroaniline. The four compounds exhibit typical aggregation-induced emission (AIE) property with relatively high solid state absolute fluorescence quantum yields (38.1–65.7%) and fast-recoverable mechanochromism property with solid-state fluorescence change between blue and yellow-green. They are thermally stable with decomposition temperatures above 319 ^{o}C. Both of multilayer electroluminescence devices fabricated with compounds **3b** and **3c** as emitters are blue emission. The turn-on voltage of device based on compound **3b** is 3.3 V with maximum luminance and current efficiency of 2470 cd/m^2 and 1.48 cd/A, respectively.

Keywords: *N*-substituted tetraphenylethene-based benzimidazoles; aggregation-induced emission; mechanochromism; electroluminescence

1. Introduction

In recent years, organic solid luminescent materials have been developed explosively due to their wide applications in organic field-effect transistors (OFETs) [1,2], organic photovoltaics (OPVs) [3-5], organic lasers [6-8] and sensors [9,10], especially in organic light-emitting diodes (OLEDs) [11-13]. In early period, aggregation-caused quenching (ACQ) effect originating from the strong π-π interaction had prevented the electronic devices application to some degree [14-17]. Consequently, the ACQ-active materials are utilized necessarily as dopants at low concentration in host materials and the devices

performance parameters depend on suitable host/dopant energy combination [18,19]. Furthermore, full-color display is closely related to red, green, and blue (RGB) tricolor emission and the performance parameters of red and green devices are excellent and constantly refreshing record. Nevertheless, there are great challenges in blue emitting device due to the defect in color purity, efficiency and life time. Hence, the synthesis of novel effective solid-state blue luminogens is still a hot topic for the researchers. Intriguingly, some solid luminogens exhibit mechanochromism property with emission change under external physical stimuli and possess potential applications in optical recording, sensors and security inks [20-22]. Mechanochromism behavior can be achieved by changing the molecular structures or solid-state molecular packing modes. The morphologic change between crystalline state and amorphous state is usually easier and reversible, which arises much attention recently.

Tetraphenylethylene (TPE) is one representative of the anti-ACQ effect molecules and the modifications of TPE have been proved an efficient way to construct new aggregation-induced emission (AIE) luminogens with high solid-state efficiencies [23-25]. As one of the commonly important modification strategies for organic optoelectronic materials, the introduction of aryl or alkyl can improve the solubility in solvent, regulate molecular packing structure, facilitate the film processing of the device and bring hypsochromic shift of emission [26-29]. Based on the above considerations, we designed and synthesized a new series of phenyl, *p*-(*tert*-butyl)phenyl and alkyl-substituted TPE-based benzimidazoles in the nitrogen position (Scheme 1). Excepting AIE-active and fast-recoverable mechanochromism bifunctional property, the introduction of substituent group in *N* position bring bluer emitting, better solubility and good film-forming ability compared with non-substituted tetraphenylethene-based benzimidazoles [30]. Then, the OLED devices using two representative compounds were fabricated. Herein, we report the syntheses, structures and properties of the new series of *N*-substituted tetraphenylethene-based benzimidazoles in detail.

Insert Scheme 1

2. Experimental

2.1 Materials and instrumentation

Tetrahydrofuran was purified by distillation from sodium and benzophenone ketyl under nitrogen condition prior to use. All other reagents and solvents were purchased commercially (AR grade) and used without further purification unless otherwise noted. The THF/water mixtures with different water

fractions were prepared by slowly adding distilled water into the THF solution of samples under ultrasound at room temperature. ^{1}H NMR and ^{13}C NMR spectra were collected on a Bruker-400 MHz spectrometer in $CDCl_3$ or DMSO solutions with TMS as an internal standard. Mass spectra were obtained on a Bruker Ultraflextreme MALDI TOF/TOF mass spectrometer and a JMS-Q1000GC MK Ⅱ Ultra Quad GC/MS. Concentrated solutions of the four compounds were drop-casted on quartz plate to prepare films, and Φ_F values of the amorphous films were determined by FM-4P-TCSPC Transient State Fluorescence Spectrometer using an integrating sphere. UV-vis spectra were recorded on Shimadzu UV-3600 with a UV-VIS-NIR spectrophotometer. Emission spectra were performed by a HITACHI fluorescence spectrometer (F-4600). Single crystal data of compounds were selected on a Bruker APEX II CCDC diffractometer with graphite monochromated Mo-Kα radiation (λ = 0.71073 Å) using the ω-scan technique. The structure was solved by direct method with the SHELXS-97 computer program, and refined by full-matrix least-squares methods (SHELXL-97) on F^2. Hydrogen atoms were added geometrically and refined using a riding model. Images were created by using DIAMOND program. CCDC numbers for complexes **3a**–**3d** are 1525826, 1535658, 1525827 and 1525828, respectively, and data can be obtained free of charge from the Cambridge Crystallographic Data Centre (CCDC) or at www.ccdc.cam.ac.uk/conts/retrieving.html. Elemental analysis (C, H, N) of the dried solid samples were carried out using an Elementary Vario El analyzer. The ground state geometries of all molecules were fully optimized using density functional theory (DFT) at the B3LYP/6-31G(d,p) level, as implemented in Gaussian 09W software package. PXRD measurements were performed by using a Bruker X-ray diffractometer (D8 Advance, Germany) with an X-ray source of Cu-Kα (λ = 0.15418 Å) at 40 kV and 40 mA at a scan rate of 4°(2θ)/min. Cyclic voltammetry experiments were performed with a CHI660A electrochemical work station. All measurements were carried out at room temperature with a conventional three-electrode configuration consisting of a glassy carbon working electrode, a platinum auxiliary electrode and a calomel reference electrode. The solvent in all experiments was dry tetrahydrofuran and the supporting electrolyte was 0.1 M tetrabutylammonium hexa-fluorophosphate. The $E_{1/2}$ values were determined as 1/2 (E_p^a + E_p^c), where E_p^a and E_p^c are the anodic and cathodic peak potentials, respectively. All potentials reported were referenced to ferrocene which was used as internal standard toward the end of each experiment. The glass-transition temperatures (T_g) of the compounds were determined with differential scanning calorimetry (DSC) under a nitrogen

atmosphere by using a DSC6000 (PerkinElmer). Samples were heated to 300 ^{o}C at a rate of 10 ^{o}C min^{-1} and cooled at 20 ^{o}C min^{-1} then heated again under the same heating conditions as used in the initial heating process. Decomposition temperatures (T_d) were determined with thermogravimetric analysis (TGA) under a nitrogen atmosphere by using a STA 449 F5 (NETZSCH). Samples were heated to 600 ^{o}C at a rate of 10 ^{o}C min^{-1}.

The devices were fabricated by vacuum deposition of the materials at 10^{-6} Torr onto indium tin oxide (ITO) glass with a sheet resistance of 25 Ω per square. Respecting to their appropriate energy levels, the OLEDs were fabricated with a typical three-layer structure of ITO/NPB (40 nm)/**3b** or **3c** (20 nm)/TPBi (40 nm)/LiF (1 nm)/Al (100 nm). The current density–voltage–luminance (*I*–*V*–*L*) characteristics were measured using a Keithley source measurement unit (Keithley 2400) with a calibrated silicon photodiode. The EL spectra of the devices were measured using a SpectraScan PR650 spectrophotometer. All measurements were carried out under air at room temperature without device encapsulation.

2.2 Synthesis

*2.2.1 General procedure for synthesis of compounds **1a**–**1d***

Under the atmosphere of nitrogen, a mixture of *ortho*-nitroaniline (5.52 g, 40 mmol), brominated compounds **a**–**b** (40 mmol), sodium *tert*-butoxide (3.84 g, 40 mmol), $Pd(dba)_2$ (0.23 g, 0.4 mmol), P(*t*-Bu)$_3$ (0.1 g mL^{-1} in toluene, 1.2 mL, 0.6 mmol) and toluene (150 mL) were heated at 80 ^{o}C for 5-6 h. After it cooled, water and dichloromethane were added and the organic layer was separated. Then, the combined organic layer was dried over $MgSO_4$. Finally, the crude products were purified by silica gel column chromatography using hexane/ethyl acetate as eluent.

Compound **1a** was obtained as a crimson oily liquid. Yield: 6.25 g, 73.0%. ^{1}H-NMR (600 MHz, d_6-DMSO) δ (ppm): 9.33 (s, 1H), 8.06 (dd, *J* = 8.5 Hz, 1.5 Hz, 1H), 7.47 – 7.42 (m, 1H), 7.37 (t, *J* = 7.9 Hz, 2H), 7.27 (d, *J* = 7.6 Hz, 2H), 7.15 (t, *J* = 7.7 Hz, 2H), 6.82 (ddd, *J* = 8.3 Hz, 7.0 Hz, 1.1 Hz, 1H). ^{13}C-NMR (151 MHz, d_6-DMSO) δ (ppm): 142.44 (s), 139.69 (s), 136.43 (s), 133.97 (s), 130.00 (s), 126.69 (s), 125.33 (s), 124.14 (s), 118.49 (s), 117.15 (s). MALDI TOF-MS: m/z 214.26 $[M]^+$.

Compound **1b** was obtained as a crimson oily liquid. Yield: 8.32 g, 77.0%.^{1}H-NMR (400 MHz, d_6-$CDCl_3$) δ (ppm): 9.48 (s, 1H), 8.19 (d, *J* = 8.6 Hz, 1H), 7.43 (d, *J* = 8.4 Hz, 2H), 7.34 (t, *J* = 7.8 Hz, 1H), 7.20 (d, *J* = 8.5 Hz, 3H), 6.74 (dd, *J* = 8.2 Hz, 7.3 Hz, 1H), 1.35 (s, 9H). ^{13}C-NMR (101 MHz, d_6-

$CDCl_3$) δ (ppm): 148.92 (s), 143.56 (s), 135.88 (s), 135.66 (s), 132.87 (s), 131.03 (s), 127.21 (s), 126.62 (d, *J* = 3.7 Hz), 124.28 (s), 117.15 (s), 116.07 (s), 34.58 (s), 31.39 (s). MALDI TOF-MS: m/z 270.21 $[M]^+$.

Compound **1c** was obtained as a crimson oily liquid. Yield: 5.82 g, 75.1%.^{1}H-NMR (400 MHz, d_6-$CDCl_3$) δ (ppm): 8.17 (d, *J* = 8.6 Hz, 1H), 8.06 (s, 1H), 7.43 (t, *J* = 7.8 Hz, 1H), 6.85 (d, *J* = 8.7 Hz, 1 H), 6.63 (dd, *J* = 8.2 Hz, 7.3 Hz, 1H), 3.30 (dd, *J* = 12.6 Hz, 6.7 Hz, 2H), 1.81 – 1.64 (m, 2H), 1.54 – 1.42 (m, 2H), 0.99 (t, *J* = 7.3 Hz, 3H). ^{13}C-NMR (101 MHz, d_6-$CDCl_3$) δ (ppm):145.65 (s), 136.18 (s), 131.68 (s), 126.90 (s), 115.01 (s), 113.77 (s), 42.73 (s), 31.00 (s), 20.25 (s), 13.79 (s). MALDI TOF-MS: m/z 194.15 $[M]^+$.

Compound **1d** was obtained as a crimson oily liquid. Yield: 6.53g, 73.5%.^{1}H-NMR (400 MHz, d_6-$CDCl_3$) δ (ppm): 8.17 (d, *J* = 8.6 Hz, 1H), 8.06 (s, 1H), 7.43 (t, *J* = 7.8 Hz, 1H), 6.84 (d, *J* = 8.7 Hz, 1H), 6.65 – 6.58 (m, 1H), 3.29 (dd, *J* = 12.5 Hz, 6.9 Hz, 2H), 1.78 – 1.68 (m, 2 H), 1.45 (dt, *J* = 14.1 Hz, 6.9 Hz, 2H), 1.35 (dt, *J* = 7.1 Hz, 3.4 Hz, 4H), 0.91 (t, *J* = 6.7 Hz, 3H). ^{13}C-NMR (101 MHz, d_6-$CDCl_3$) δ (ppm): 145.65 (s), 136.18 (s), 131.68 (s), 126.90 (s), 115.00 (s), 113.77 (s), 77.34 (s), 77.02 (s), 76.70 (s), 43.05 (s), 31.47 (s), 28.92 (s), 26.75 (s), 22.56 (s), 14.01 (s). MALDI TOF-MS: m/z 222.19 $[M+1]^+$.

*2.2.2 Synthesis of compound **2***

Compound **2** was prepared according to the reported synthetic route and obtained as a yellowish powder solid [31]. ^{1}H-NMR (400 MHz, d_6-DMSO) δ (ppm): 9.86 (s, 1H), 7.66 (d, *J* = 8.2 Hz, 2H), 7.20-7.06 (m, 11H), 7.00 (ddd, *J* = 7.4 Hz, 3.9 Hz, 1.9 Hz, 6H). ^{13}C-NMR (101 MHz, d_6-DMSO) δ (ppm): 150.12 (s), 142.95 (dd, *J* = 25.1 Hz, 11.1 Hz), 140.05 (s), 134.59 (s), 131.86 (s), 131.07 (d, *J* = 8.6 Hz), 129.52 (s), 128.77-128.02 (m), 127.41 (d, *J* = 14.1 Hz). GC/MSD: m/z 360 $[M]^+$.

*3.2.3 General procedure for syntheses of compounds **3a–3d***

Under room temperature, $Na_2S_2O_4$ (1.4 g, 8 mmol) was added in batches to a solution of compounds **1** (2 mmol) and **2** (0.72 g, 2 mmol) in MeCN/water (50/10 mL), then the mixed solution was heated to reflux for 12 h. After completion of the reaction, the reaction mixture was quenched by pouring into ice water. The organic layer was extracted with dichloromethane, and the combined organic layers were washed with a saturated brine solution and water, and dried over $MgSO_4$. After filtration and solvent evaporation, the crude product was purified by silica-gel column chromatography using hexane/ethyl

acetate as eluent.

Compound **3a** was obtained as a white powder solid. Yield: 0.70 g, 67.0%.^{1}H-NMR (400 MHz, d_6-DMSO) δ (ppm): 7.75 (d, *J* = 7.9 Hz, 1H), 7.54 (m, 3H), 7.35 (d, *J* = 7.0 Hz, 2H), 7.28 (m, 4H), 7.18 – 7.09 (m, 10H), 7.00 – 6.90 (m, 8H). ^{13}C-NMR (101 MHz, d_6-$CDCl_3$) δ (ppm): 152.30 (s), 145.06 (s), 143.22 (dd, *J* = 30.5 Hz, 11.2 Hz), 141.83 (s), 140.12 (s), 137.03 (d, *J* = 14.9 Hz), 131.61 – 130.61 (m), 129.72 (s), 128.74 (s), 128.41 (s), 127.70 (dd, *J* = 6.1 Hz, 4.3 Hz), 127.32 (s), 126.62 (d, *J* = 6.3 Hz), 123.07 (d, *J* = 29.7 Hz), 119.73 (s), 110.34 (s). MALDI TOF-HRMS: m/z 524.1883 $[M]^+$. Anal. Calcd for $C_{39}H_{28}N_2$: C, 89.28; H, 5.38; N, 5.34. Found: C, 89.31; H, 5.37; N, 5.32.

Compound **3b** was obtained as a white powder solid. Yield: 0.85 g, 73.4%.^{1}H-NMR (400 MHz, d_6-DMSO) δ (ppm): 7.74 (d, *J* = 7.8 Hz, 1H), 7.55 (d, *J* = 8.4 Hz, 2H), 7.32 – 7.20 (m, 6H), 7.19 – 7.09 (m, 10H), 7.01 – 6.88 (m, 8H), 1.35 (s, 9H). ^{13}C-NMR (101 MHz, d_6-$CDCl_3$) δ (ppm): 152.29 (s), 151.50 (s), 144.94 (s), 143.26 (dd, *J* = 35.1, 16.6 Hz), 141.70 (s), 140.17 (s), 137.26 (s), 134.17 (s), 131.31 (dd, *J* = 11.6 Hz, 5.8 Hz), 128.72 (s), 127.78 (d, *J* = 26.5 Hz), 126.62 (dd, *J* = 11.5 Hz, 4.8 Hz), 122.93 (d, *J* = 27.3 Hz), 119.64 (s), 110.53 (s), 34.79 (s), 31.36 (s). MALDI TOF-HRMS: m/z 581.3379 $[M+1]^+$. Anal. Calcd for $C_{43}H_{36}N_2$: C, 88.93; H, 6.25; N, 4.82. Found: C, 88.92; H, 6.28; N, 4. 73.

Compound **3c** was obtained as a white powder solid. Yield: 0.75 g, 74.8%.^{1}H-NMR (400 MHz, d_6-DMSO) δ (ppm): 7.63 (t, *J* = 7.3 Hz, 2H), 7.54 (d, *J* = 8.1 Hz, 2H), 7.29 – 7.12 (m, 13H), 7.03 (dd, *J* = 12.3 Hz, 6.4 Hz, 6H), 4.24 (t, *J* = 7.2 Hz, 2H), 1.62 – 1.51 (m, 2H), 1.07 (dd, *J* = 14.5 Hz, 7.2 Hz, 2H), 0.72 (t, *J* = 7.2 Hz, 3H). ^{13}C-NMR (101 MHz, d_6-DMSO) δ (ppm): 153.13 (s), 145.01 (s), 143.90 – 142.77 (m), 141.93 (s), 140.38 (s), 136.04 (s), 131.21 (dd, *J* = 17.9 Hz, 14.9 Hz), 129.05 (s), 128.39 (d, *J* = 9.0 Hz), 127.22 (s), 122.58 (d, *J* = 47.3 Hz), 119.52 (s), 111.27 (s), 44.01 (s), 31.45 (s), 19.55 (s), 13.74 (s). MALDI TOF-HRMS: m/z 505.2631 $[M+1]^+$. Anal. Calcd for $C_{37}H_{32}N_2$: C, 88.06; H, 6.39; N, 5.55. Found: C, 88.10; H, 6.37; N, 5.53.

Compound **3d** was obtained as a white powder solid. Yield: 0.76 g, 71.5%.^{1}H-NMR (400 MHz, d_6-DMSO) δ (ppm): 7.66 – 7.58 (m, 2H), 7.53 (d, *J* = 8.0 Hz, 2H), 7.30 – 7.11 (m, 13H), 7.03 (dd, *J* = 9.2 Hz, 5.2 Hz, 6H), 4.23 (t, *J* = 7.3 Hz, 2H), 1.58 (dd, *J* = 14.2 Hz, 7.1 Hz, 2H), 1.10 (ddd, *J* = 23.1 Hz, 13.9 Hz, 7.6 Hz, 6H), 0.78 (t, *J* = 6.9 Hz, 3H). ^{13}C-NMR (101 MHz, d_6-DMSO) δ (ppm): 153.11 (s), 144.97 (s), 143.26 (dd, *J* = 27.4 Hz, 14.2 Hz), 141.93 (s), 140.37 (s), 136.07 (s), 131.21 (dd, *J* = 17.7

Hz, 13.3 Hz), 129.05 (d, *J* = 9.9 Hz), 128.37 (d, *J* = 8.4 Hz), 127.22 (s), 122.57 (d, *J* = 48.1 Hz), 119.53 (s), 111.25 (s), 44.34 (s), 30.87 (s), 29.27 (s), 25.94 (s), 22.33 (s), 14.21 (s). MALDI TOF-HRMS: m/z 533.2947 $[M+1]^+$. Anal. Calcd for $C_{39}H_{36}N_2$: C, 87.93; H, 6.81; N, 5.26. Found: C, 87.91; H, 6.82; N, 5.27.

3. Results and discussion

3.1 Synthesis and characterization

The synthetic procedures of the four compounds are shown in Scheme 2. Compounds **1a**–**1d** were synthesized by *N*-substituted reaction with starting materials *ortho*-nitroaniline [32]. Another key reactant 4-tetraphenylenthenealdehyde (**2**) was obtained according to the conventional method of literature [31]. Then, target compounds **3a**–**3d** were one-pot synthesized by the cyclization reaction of the intermediate **2** with *ortho*-nitroaniline derivatives in high yields. These compounds were purified by column chromatography followed by recrystallization then characterized by standard spectroscopic methods, from which satisfactory analysis data corresponding to these compounds were obtained. Moreover, the final compounds **3a**–**3d** were also characterized by single crystal X-ray diffraction analysis. Generally, four new *N*-substituted TPE-based benzimidazoles have been synthesized conveniently based on 4-tetraphenylenthenealdehyde.

Insert Scheme 2

*3.2 Crystal structures of compounds **3a**–**3d***

Insert Fig. 1

Single X-ray diffraction analysis is a good way to better understand the relationship between the properties and structures. Successfully, the single crystals of compounds **3a**–**3d** were obtained by the solvent evaporation method in tetrahydrofuran/water (**3a**–**3b**) and ethyl acetate/n-hexane (**3c**–**3d**) mixture. As depicted in Fig. 1, the crystal structures of the four compounds agree well with the expected molecular structures. The four compounds all show highly twisted paddle-shaped conformations, which are similar to the reported TPE-based compounds [33,34]. In compounds **3a**–**3d**, the benzimidazole segments are connected to the benzene rings of TPE unit with the torsion angles of 44.20°, 34.62°, –41.87° and 39.25°, respectively.

As expected, there are not relatively strong π-π and N-H---N intermolecular interactions in the

crystal structures of the four compounds. There are affluent weak C-H---π and C-H---N intermolecular interactions which link the molecules of compounds **3a**-**3d** to form two-dimensional (2D) layer-like supramolecular structures (Fig. S1). Then, all the four compounds adopt a fashion stacking by 2D layers to form three-dimensional (3D) structures (Fig. S2). As a result, there exist interface gaps without any intersections between adjacent two layers. Therefore, under external pressure, the layers can slip readily and the highly ordered crystal structures are destroyed, which can be responsible for the mechanochromism phenomenon of the four compounds.

Insert Fig. 2

As shown in Fig. 2 and Fig. S1, the packing diagrams of these compounds show affluent weakly intermolecular interactions. For compound **3a**, there are five C-H---π interactions between hydrogen atoms and the π clouds of phenyl rings in adjacent molecules with distances of 2.722–2.949 Å and one C-H---N(2) interactions between N(2) atom of benzimidazole and hydrogen atom on phenyl ring attaching to the N(1) atom of benzimidazole in adjacent molecule with a distance of 2.636 Å. For compound **3b**, there exists three C-H---π interactions between hydrogen atoms and the π clouds of phenyl rings in adjacent molecules with distances of 2.779–3.272 Å and one C-H---N(2) interactions between N(2) atom of benzimidazole and hydrogen atom on phenyl ring of TPE unit in adjacent molecule with a distance of 2.378 Å. In packing diagram of compound **3c**, there exist six C-H---π interactions between hydrogen atoms on phenyl rings or *n*-butyl and the π clouds of phenyl rings in adjacent molecules with distances of 2.701–3.117 Å. For compound **3d**, there exists five C-H---π interactions between hydrogen atoms on phenyl rings or *n*-hexyl and the π clouds of phenyl rings in adjacent molecules with a distance of 2.806–3.011 Å, one C-H---N(2) interaction between N(2) atom of benzimidazole and hydrogen atom on phenyl ring of TPE segment in adjacent molecules with a distance of 2.638 Å and the only π-π intermolecular interactions between phenyl rings of TPE in adjacent molecules with distances of 3.273 Å. The affluent intermolecular interactions in the crystal structures of compounds **3a**–**3d** contribute to restrict the molecular rotations of C-C single bond in the solid state, reduce the non-radiative transition consumption and further facilitate the fluorescence emission.

3.3 Photophysical properties

The UV-visible spectra and solid emission spectra of the four compounds are demonstrated in Fig. 3a, 3b and Fig.S4, respectively. Compounds **3a**–**3d** exhibit similar absorption behavior with two major absorption band at 270–310 nm and 310–400 nm, respectively (Fig. 3a). The former absorption band corresponds to the π-π* electronic transition of the molecule skeleton. TPE and imidazole segment are weak electron donor and acceptor, respectively, the latter long region absorption band is attributed to charge transfer (CT) from the TPE core to imidazole segment, which can be compared with other some N-containing compounds [35-37]. To study the solvent-dependent properties of the four compounds, we choose compound **3d** as an representative and measure the absorption spectra in different polar solvents such as n-hexane (HEX), dichloromethane (DCM), acetonitrile (MeCN), methanol (MeOH) and dimethyl sulfoxide (DMSO). As displayed in Fig. S3, slight red-shift is found for compound **3d**, which is in accordance with theory calculations, suggesting weak CT characteristics and poor CT efficiency due to large torsion angles between benzimidazole segments and the conjoint benzene rings of TPE unit. The absorption maxima of compounds **3a** and **3b** show a slight bathochromic shift compared with those of compounds **3c** and **3d,** which was attributed to the enlargement of π-π conjugation with introduction of phenyl group. As shown in Fig. 3b, the corresponding emission peaks of compounds **3a**–**3d** appear at 448, 454, 440 and 446 nm, respectively. The solid photoluminescence (PL) spectra of these four compounds display relatively blue shift (in the range of 11 nm to 25 nm) compared to the compounds without substituent group in the benzimidazole unit [30]. This may be attributed to twisted molecular conformation disclosing their shorter π-conjugation lengths and weakening intermolecular interactions especially π-π interactions [38]. The measurements of the absolute fluorescence quantum yields (Φ_F) in crystalline state reveal that all of the compounds are strong solid state emitters with the Φ_F values of 38.1% for **3a**, 54.6% for **3b**, 60.4% for **3c** and 65.7% for **3d**, respectively. The fluorescence quantum yields of compounds **3c** and **3d** are significantly larger than those of **3a** and **3b**, which can be due to that the phenyl ring attached to benzimidazole segment is favorable for the formation of C-H---N and C-H---π intermolecular interactions, which can reduce the fluorescence emission. In addition, the fluorescence quantum yield of **3b** is higher than that of compound **3a** and the same for compound **3d** is higher than that of compound **3c**, which may be attributed to the *tert*-butyl group and the longer hexyl chain increase the steric hindrance in solid state.

Insert Fig. 3

Insert Table 1

The AIE behaviors of **3a**–**3d** were studied by PL spectra in THF–water mixtures with different water fractions (f_w). Compounds **3a**–**3d** are highly soluble in THF and weakly emissive, invisible particulates formed by increasing the water fraction in THF/water mixtures, leading to the change in PL spectra. Compounds **3a**–**3d** are weakly fluorescent when the f_w value is lower than 75%. After that, with increasing f_w, all the PL intensity of compounds **3a**–**3d** fast increases monotonously until the measured f_w up to 95% (Fig. 3c and Fig. S4). The results of PL spectra demonstrate that all these compounds display weak emission in THF, but exhibit intense emission in their aggregate state. This phenomenon demonstrates that these four compounds are AIE-active and the invisible particulates fast assemble in a constant fashion with the increase of f_w. The restriction of intramolecular rotation (RIR) may account for the different emission behaviors between their solution and aggregate state [39]. The faint fluorescence in THF is enhanced in the aggregated suspension (f_w = 95%) by 403-, 410-, 314- and 393-fold for compounds **3a**–**3d**, respectively (Fig. 3d).

3.4 Mechanochromic properties

The mechanochromic properties of compounds **3a**–**3d** were studied by solid state emission spectroscopy and the data are summarized in Table 1. Compounds **3a**–**3d** show blue emission with wavelengths ranging from 440 nm to 454 nm in their crystalline states. Upon grinding using a spatula or a pestle, the blue emitting solids can convert to yellowish green emitting solids and the emission wavelength is red-shifted to a range from 463 nm to 481 nm (Fig. 4a and Fig. S5). The compounds **3a**–**3d** show grinding−induced spectral red shift ($\Delta\lambda$) of 21 nm, 29 nm, 23 nm and 26 nm, respectively. After the ground samples of these four compounds are fumed with DCM vapor, the PL wavelengths rapidly blue-shift to their original state completely within a few seconds and keep stable, indicating that the four compounds have perfect restorability with high sensitivity comparing to other reported mechanochromic compounds [40-42]. The absence of hydrogen bonding interaction leads to better solubility in organic solvent such as DCM resulted from the introduction of peripheral aryl and alkyl substituents in the nitrogen position. This may be the main reason for these compounds sensitive to warm solvent vapor. After several grinding-fuming cycles, the PL wavelength has no obvious abnormal changes demonstrating excellent stability (Fig. S6). Given the sensitivity and stability, these

compounds have the potential application in organic vapor sensor.

Compounds **3a**–**3d** at different solid states were studied by powder X-ray diffraction (PXRD) to investigate mechanochromism phenomenon (Fig. 4b and Fig. S5). The diffraction patterns of compounds **3a**–**3d** in pristine solid state show sharp peaks, illustrating the crystalline state of morphology. After grinding, the PXRD results of these compounds show very weak diffraction signal intensity or a broad diffuse band, indicating that the morphology change from crystalline state to amorphous state. The PXRD spectra of ground compounds **3a**–**3d** return to display sharp peaks after fumed with DCM vapor and these peaks coincide with those of as-prepared crystals, demonstrating restorability of morphology from amorphous state to crystalline state. The PXRD study illustrates that the morphological change from the crystalline state to the amorphous state and vice versa is related to the mechanochromism in compounds **3a**–**3d**.

The single crystal structures and PXRD of the compounds **3a**–**3d** demonstrate the relationship between solid packing structure and mechanochromic property. Due to interface gaps existing between two adjacent layers, the crystal ordered packing structures can be destroyed under external pressure, which can bring to the planarization of molecular conformation [43,44], results in the increase of the effective molecular conjugation effects and further leads to a red-shift of emissions.

Insert Fig. 4

Insert Table 2

3.5 Theoretical calculation and electrochemical studies

We performed quantum mechanical computations by density functional theory (DFT) calculations using the Gaussian 09W software to further understand the correlation between structure and the physical properties. The DFT calculations were performed at the B3LYP/6-31G(d,p) level of theory. The optimized molecular structures of those compounds are shown in Fig. S7. The benzimidazole segments are connected to the benzene rings of TPE unit with the torsion angles of 27.4°, 28.6°, –40.7° and 41.6°, respectively. Torsion angles of compounds **3c** and **3d** are similar to that of crystal structure. However, for compounds **3a** and **3b**, torsion angles calculated by DFT method are smaller compared with that of their crystal structure. DFT calculations illustrates that benzimidazole segment and conjoint benzene rings of compounds **3a** and **3b** in ideal condition is close to coplanarity and benefit to

electronic cloud movement from TPE unit to benzimidazole segment. The contours of the highest occupied molecular orbital (HOMO) and lowest unoccupied molecular orbital (LUMO) of **3a**–**3d** are shown in Fig. S7. Electronic distributions observed from the frontier orbitals of compounds **3a**–**3d** are approximately identical. The electron clouds of HOMO levels are located on the whole molecule except the *N*-substituted groups, which indicates peripheral substituents have a little influence on HOMO levels. LUMO levels of the compounds mainly distributed at the imidazole segment and the conjoint benzene ring of TPE, demonstrating weak intramolecular charge transfer. The theoretical band gaps for **3a**–**3d** are 3.81 eV, 3.81 eV, 3.90 eV and 3.90 eV, respectively (Table. 2).

The cyclic voltammetry (CV) measurement was performed to investigate electrochemical properties of the four compounds in anhydrous THF with the concentration of 1.0×10^{-4} M (Fig. 5) and the corresponding data are summarized in Table 2. On the basis of the onset potentials of oxidation (E^{ox}_{onset}), the HOMO energy levels of these compounds were calculated with the values of 5.47, 5.42, 5.43 and 5.44 eV, respectively, using the equation HOMO = $-eE_{onset} - 4.31$ eV. From the edge in absorption spectra, the band gaps were acquired with the values of 3.17 eV for **3a**, 3.17 eV for **3b**, 3.22 eV for **3c** and 3.22 eV for **3d**. The LUMO values of the four compounds can be obtained by subtraction of the optical band gap energies from the HOMO energy levels with the values of 2.30, 2.25, 2.21 and 2.22 eV, respectively.

Insert Fig. 5

3.6 Thermal properties

As shown in Fig. 6, the thermal properties of compounds **3a**–**3d** were investigated by thermogravimetric (TGA) and differential scanning calorimetry (DSC) analyses. These compounds show high thermal decomposition (T_d) temperatures with the values of 348, 351, 319 and 340 ^oC for compounds **3a**–**3d**, respectively. As shown in Fig. 6b, glass transition temperatures (T_g) of compounds **3a** and **3b** are relatively high with T_g values of 87.6 and 91.1 ^oC, respectively. However, compounds **3c** and **3d** have poor performance with the T_g values of 53.8 and 40.5 ^oC. The T_d and T_g values of compounds **3a** and **3b** are higher than those of compounds **3c** and **3d**, indicating that the introduction of phenyl and *p*-(*tert*-butyl)phenyl group is better than alkyl group to improve thermostability. The T_d value of compound **3d** is higher than that of compound **3c**, while the T_g value of compound **3d** is lower

than that of compound **3c**, which illustrates that increasing the length of alkyl chain enhances thermal property but decreases glass transition temperature. In addition, compound **3a** shows obvious cold-crystallization peak and corresponding crystal melting peak, which indicates that compounds **3b**–**3d** changing from glassy state to crystalline state are difficult. As shown in Fig. S8, different from pristine crystal samples, the DSC curve of the ground powder of the four compounds show a broad exothermic peak before melting, revealing that the ground samples are in a metastable amorphous state and can crystallize in the solid state upon heating. It illustrates that the molecular packing patterns of compounds **3a**–**3d** can transform from the crystalline to the amorphous state by grinding.

Insert Fig. 6

3.7 Electroluminescence

Owing to their relatively high absolute fluorescence quantum yields and glass transition temperatures, non-doped OLED devices based on compounds **3b** and **3c** were fabricated with a typical configuration of ITO/NPB (40 nm)/**3b** or **3c** (20 nm)/TPBi (40 nm)/LiF (1 nm)/Al (100 nm) without optimized, where the new luminogens serve as emitters, NPB was used as hole-transporting layer and TPBi was used as electron-transporting layer. The devices performances were summarized in Table 3. Fig. 7a and 7b plot the current density–voltage–luminance (*I*–*V*–*L*) characteristics of the OLED devices **I** (**3b)** and **II** (**3c**), respectively. The turn-on voltage (V_{on}) of device **I** was at 3.3 V, by contrast, the V_{on} of device **II** was higher with value of 4.8 V. The lower V_{on} value suggests the less dissipation of energy associated with carrier injection or transportation. For device **I**, it has the maximum luminance efficiency and power efficiency of 1.48 cd/A and 1.05 lm/W, respectively, yielding a maximum luminance of 2470 cd m^{-2} at 6.8 V. Device **II** performed dissatisfactory with a maximum luminance of 843 cd cm^{-2} at 7.8 V and the maximum luminance efficiency and power efficiency of the device are 2.28 cd/A and 1.12 lm/W, respectively. Both devices exhibit blue emission with maximum emission peaks at 436 nm, 432 nm and the CIE coordinates of the devices are (0.180, 0.171) and (0.179, 0.149), respectively (Fig. S9). The EL spectra of compounds **3b** and **3c** are blue lighting, which are close to their crystal solid PL spectra. Besides, the PL spectra of the vacuum deposited films of compounds **3b** and **3c** are sky blue emission (Fig. S10). Therefore, the molecule stacking of compounds **3b** and **3c** in device **I** and **II** may be nearly to their crystal state. As the literature reported, crowded and twisted conformation will

encourage the formation of the crystalline state in the thin films in OLED devices [45]. However, plenty of luminescent materials in OLED devices exist as amorphous state and the EL spectra are bathochromic-shifted compared to PL spectra of crystal solid [23,45-47]. Of course, the actual molecule stacking of luminescent materials in OLED devices depends on many factors such as the structural nature of materials and the fabricating conditions of devices. The results herein indicate that *N*-substituted tetraphenylethene-based benzimidazoles herein are suitable for OLEDs compared with their non-substituted precursors as expected in molecular design of Scheme 1. Therefore, the reasonable modification based on TPE and its derivatives is still one effective strategy for new OLED materials.

Insert Table 3

Insert Fig. 7

4 Conclusions

In summary, we have designed and synthesized a new series of blue-emitting *N*-substituted tetraphenylethene-based benzimidazoles (**3a**–**3d**). All the compounds are typical AIE-active compounds with relatively excellent absolute fluorescence quantum yields (38.1-65.7%) and high thermal stability. These compounds exhibit reversible mechanochromism behaviors under external pressure and DCM vapor with emission changes between blue and yellow-green. Their single crystal structures demonstrate that crystal packing structures can be destroyed due to interfaces gaps between layers exists in unconsolidated molecular packing structures. The PXRD results confirm that the transformation of the twisted crystalline state to the planar amorphous state is related to mechanochromism behaviors in the compounds **3a**–**3d**. Multilayer OLEDs are fabricated using compounds **3b** and **3c** as emitting layer, which emit blue light. The OLED based on compound **3b** shows a better performance with the lower turn-on voltage of 3.3 V and maximum luminance of 2470 cd m^{-2}. Both OLEDs are blue emission which have the potential application in flat panel display as blue-light emitting materials and provide a reference for designing excellent blue-emitting molecules in solid state.

Acknowledgements

This work was supported by the Fundamental Research Funds for the Central Universities

(2015XKZD08) and the Priority Academic Program Development of Jiangsu Higher Education Institutions.

References

[1] Yuen J D, Fan J, Seifter J, Lim B, Hufschmid R, Heeger A J, Wudl F. High performance weak donor–acceptor polymers in thin film transistors: effect of the acceptor on electronic properties, ambipolar conductivity, mobility, and thermal stability. J Am Chem Soc 2011; 133: 20799-807.

[2] O Neill M, Kelly S M. Ordered materials for organic electronics and photonics. Adv Mater 2011; 23: 566-84.

[3] Wang N N, Yu J S, Zheng Y F, Guan Z Q, Jiang Y D. Organic photovoltaic cells based on a medium-bandgap phosphorescent material and c60. J Phys Chem C 2012; 116: 5887-91.

[4] Ma S Y, Fu Y Y, Ni D B, Mao J, Xie Z Y, Tu G L. Spiro-fluorene based 3d donor towards efficient organic photovoltaics. Chem Commun 2012; 48: 11847-49.

[5] Thompson B C, Fréchet J M J. Polymer–fullerene composite solar cells. Angew Chem Int Edit 2008; 47: 58-77.

[6] Fan H H, Guo L, Li K F, Wong M S, Cheah K W. Exceptionally strong multiphoton-excited blue photoluminescence and lasing from ladder-type oligo(*p*-phenylene)s. J Am Chem Soc 2012; 134: 7297-300.

[7] Görrn P, Lehnhardt M, Kowalsky W, Riedl T, Wagner S. Elastically tunable self-organized organic lasers. Adv Mater 2011; 23: 869-72.

[8] Kim H, Schulte N, Zhou G, Müllen K, Laquai F. A high gain and high charge carrier mobility indenofluorene-phenanthrene copolymer for light amplification and organic lasing. Adv Mater 2011; 23: 894-97.

[9] Zhu L N, Qin J G, Yang C L. New metal-coordination-inhibited charge transfer emission for terfluorenes: highly sensitive and selective detection for Hg^{2+} with ratiometric “turn-on” fluorescence response. Chem Commun 2009; 46: 8755-7.

[10] Nie J, Li N, Ni Z H, Zhao Y, Zhang L F. A sensitive tetraphenylethene-based fluorescent probe for Zn^{2+} ion involving ESIPT and CHEF processes. Tetrahedron Lett 2017; 58: 1980-4.

[11] Chua M H, Huang K W, Xu J W, Wu J S. Unusual intramolecular hydrogen transfer in 3,5-di(triphenylethylenyl) BODIPY synthesis and 1,2-migratory shift in subsequent scholl type

reaction. Org Lett 2015; 17: 4168-71.

[12] Qin W, Lam J W Y, Yang Z Y, Chen S M, Liang G D, Zhao W J, Kwok H S, Tang B Z. Red emissive AIE luminogens with high hole-transporting properties for efficient non-doped oleds. Chem Commun 2015; 51: 7321-4.

[13] Kim J Y, Yasuda T, Yang Y S, Adachi C. Bifunctional star-burst amorphous molecular materials for OLEDs: achieving highly efficient solid-state luminescence and carrier transport induced by spontaneous molecular orientation. Adv Mater 2013; 25: 2666-71.

[14] Wu K C, Ku P J, Lin C S, Shih H T, Wu F I, Huang M J, Lin J J, Chen I C, Cheng C H. The photophysical properties of dipyrenylbenzenes and their application as exceedingly efficient blue emitters for electroluminescent devices. Adv Funct Mater 2008; 18: 67-75.

[15] Moorthy J N, Natarajan P, Venkatakrishnan P, Huang D, Chow T J. Steric inhibition of π-stacking: 1,3,6,8-tetraarylpyrenes as efficient blue emitters in organic light emitting diodes (OLEDs). Org Lett 2007; 9: 5215-8.

[16] Jakubiak R, Collison C J, Wan W C, Rothberg L J, Hsieh B R. Aggregation quenching of luminescence in electroluminescent conjugated polymers. J Phys Chem A 1999; 103: 2394-8.

[17] Berlman I B. On an empirical correlation between nuclear conformation and certain fluorescence and absorption characteristics of aromatic compounds. J Phys Chem 1970; 74: 3085-93.

[18] Zhang R, Zhang T F, Xu L, Han F F, Zhao Y, Ni Z H. A new series of short axially symmetrically and asymmetrically 1,3,6,8-tetrasubstituted pyrenes with two types of substituents: syntheses, structures, photophysical properties and electroluminescence. J Mol Struct 2017; 1127: 237-46.

[19] Wee K R, Ahn H C, Son H J, Han W S, Kim J E, Cho D W, Kang S O. Emission color tuning and deep blue dopant materials based on 1,6-bis(*N*-phenyl-*p*-(*R*)-phenylamino)pyrene. J Org Chem 2009; 74: 8472-5.

[20] Wang X Q, Liu Q S, Yan H, Liu Z P, Yao M G, Zhang Q F, Gong S W, He W J. Piezochromic luminescence behaviors of two new benzothiazole-enamido boron difluoride complexes: intra- and inter-molecular effects induced by hydrostatic compression. Chem Commun 2015; 51: 7497-500.

[21] Luo X, Zhao W, Shi J, Li C, Liu Z, Bo Z, Dong Y Q, Tang B Z. Reversible switching emissions of tetraphenylethene derivatives among multiple colors with solvent vapor, mechanical, and thermal

stimuli. J Phys Chem C 2012; 116: 21967-72.

[22] Sase M, Yamaguchi S, Sagara Y, Yoshikawa I, Mutai T, Araki K. Piezochromic luminescence of amide and ester derivatives of tetraphenylpyrene—role of amide hydrogen bonds in sensitive piezochromic response. J Mater Chem 2011; 21: 8347-54.

[23] Chan C Y K, Lam J W Y, Zhao Z J, Chen S M, Lu P, Sung H H Y, Kwok H S, Ma Y G, Williams I D, Tang B Z. Aggregation-induced emission, mechanochromism and blue electroluminescence of carbazole and triphenylamine-substituted ethenes. J Mater Chem C 2014; 2: 4320-7.

[24] Jadhav T, Choi J M, Lee J Y, Dhokale B, Misra R. Non-doped blue organic light emitting devices based on tetraphenylethylene-π-imidazole derivatives. Org Electron 2016; 37: 448-52.

[25] Jadhav T, Dhokale B, Patil Y, Mobin S M, Misra R. Multi-stimuli responsive donor–acceptor tetraphenylethylene substituted benzothiadiazoles. J Phys Chem C 2016; 120: 24030-40.

[26] Zhang Y, Lai S L, Tong Q X, Lo M F, Ng T W, Chan M Y, Wen Z C, He J, Jeff K S, Tang X L, Liu W M, Ko C C, Wang P F, Lee C S. High efficiency nondoped deep-blue organic light emitting devices based on imidazole-π-triphenylamine derivatives. Chem Mater 2012; 24: 61-70.

[27] Kumar N S S, Varghese S, Suresh C H, Rath N P, Das S. Correlation between solid-state photophysical properties and molecular packing in a series of indane-1,3-dione containing butadiene derivatives. J Phys Chem C 2009; 113: 11927-35.

[28] Ho M H, Wu Y S, Wen S W, Lee M T, Chen T M. Highly efficient deep blue organic electroluminescent device based on 1-methyl-9,10-di(1-naphthyl)anthracene. Appl Phys Lett 2006; 89: 252903.

[29] Thiery S, Tondelier D, Declairieux C, Seo G, Geffroy B, Jeannin O, Rault-Berthelot J, Métivier R, Poriel C. 9,9′-spirobifluorene and 4-phenyl-9,9′-spirobifluorene: pure hydrocarbon small molecules as hosts for efficient green and blue PhOLEDs. J Mater Chem C 2014; 2: 4156-66.

[30] Zhang T F, Zhang R, Zhang Z M, Ni Z H. A series of tetraphenylethene-based benzimidazoles: syntheses, structures, aggregation-induced emission and reversible mechanochromism. Rsc Adv 2016; 6: 79871-8.

[31] Zhao N, Yang Z Y, Lam J W Y, Sung H H Y, Xie N, Chen S J, Su H M, Gao M, Williams I D, Wong K S, Tang B Z. Benzothiazolium-functionalized tetraphenylethene: an AIE luminogen with tunable solid-state emission. Chem Commun 2012; 48: 8637-9.

[32] Zhang R, Zhao Y, Zhang T F, Xu L, Ni Z H. A series of short axially symmetrically 1,3,6,8-tetrasubstituted pyrene-based green and blue emitters with 4-*tert*-butylphenyl and arylamine attachments. Dyes Pigments 2016; 130: 106-15.

[33] Zhang Z M, Zhao Y, Zhang R, Zhang L F, Cheng W Q, Ni Z H. Design and synthesis of a new series of tetra(polycyclic aryl)ethenes: achieving aggregation-induced emission and efficient solid-state photoluminescence. Dyes Pigments 2015; 118: 95-101.

[34] Chen L, Jiang Y B, Nie H, Hu R R, Kwok H S, Huang F, Qin A J, Zhao Z J, Tang B Z. Rational design of aggregation-induced emission luminogen with weak electron donor-acceptor interaction to achieve highly efficient undoped bilayer OLEDs. Acs Appl Mater Inter 2014; 6: 17215-25.

[35] Chen L, Lin G W, Peng H R, Nie H, Zhuang Z Y, Shen P C, Ding S Y, Huang D J, Hu R R, Chen S M, Huang F, Qin A J, Zhao Z J, Tang B Z. Dimesitylboryl-functionalized tetraphenylethene derivatives: efficient solid-state luminescent materials with enhanced electron-transporting ability for nondoped OLEDs. J Mater Chem C 2016; 4: 5241-7.

[36] Shi H P, Li M, Fang L, Dong X Q, Zhang X L, Peng H R, Chen S M, Tang B Z. Synthesis, aggregation-induced emission, and electroluminescence properties of a novel emitter comprising tetraphenylethene and carbazole moieties. Synthetic Met 2016; 220: 356-61.

[37] Li R H, Xiao S Z, Li Y, Lin Q F, Zhang R H, Zhao J, Yang C Y, Zou K, Li D S, Yi T. Polymorphism-dependent and piezochromic luminescence based on molecular packing of a conjugated molecule. Chem Sci 2014; 5: 3922-8.

[38] Huang J, Sun N, Chen P Y, Tang R L, Li Q Q, Ma D G, Li Z. Largely blue-shifted emission through minor structural modifications: molecular design, synthesis, aggregation-induced emission and deep-blue OLED application. Chem Commun 2014; 50: 2136-8.

[39] Li Z, Dong Y Q, Mi B X, Tang Y H, Häussler M, Tong H, Dong Y P, Lam J W Y, Ren Y, Sung H H Y, Wong K S, Gao P, Williams I D, Kwok H S, Tang B Z. Structural control of the photoluminescence of silole regioisomers and their utility as sensitive regiodiscriminating chemosensors and efficient electroluminescent materials. J Phys Chem B 2005; 109: 10061-6.

[40] Jadhav T, Dhokale B, Patil Y, Misra R. Aggregation induced emission and mechanochromism in tetraphenylethene substituted pyrazabole. Rsc Adv 2015; 5: 68187-91.

[41] Jadhav T, Dhokale B, Mobin S M, Misra R. Aggregation induced emission and mechanochromism

in pyrenoimidazoles. J Mater Chem C 2015; 3: 9981-8.

[42] Gao H Z, Xu D F, Liu X L, Han A X, Zhou L, Zhang C, Li Z, Dang J. Tetraphenylethene-based *β*-diketonate boron complex: efficient aggregation-induced emission and high contrast mechanofluorochromism. Dyes Pigments 2017; 139: 157-65.

[43] Gong Y Y, Tan Y Q, Liu J, Lu P, Feng C F, Yuan W Z, Lu Y W, Sun J Z, He G F, Zhang Y M. Twisted D-π-A solid emitters: efficient emission and high contrast mechanochromism. Chem Commun 2013; 49: 4009-11.

[44] Xu B J, Chi Z G, Zhang J Y, Zhang X Q, Li H Y, Li X F, Liu S W, Zhang Y, Xu J R. Piezofluorochromic and aggregation-induced-emission compounds containing triphenylethylene and tetraphenylethylene moieties. Chem-Asian J 2011; 6: 1470-8.

[45] Huang J, Sun N, Yang J, Tang R L, Li Q Q, Ma D G, Qin J G, Li Z. Benzene-cored fluorophors with tpe peripheries: facile synthesis, crystallization-induced blue-shifted emission, and efficient blue luminogens for non-doped OLEDs. J Mater Chem 2012; 22: 12001-7.

[46] Cui Y, Yin Y M, Cao H T, Zhang M, Shan G G, Sun H Z, Wu Y, Su Z M, Xie W F. Efficient piezochromic luminescence from tetraphenylethene functionalized pyridine-azole derivatives exhibiting aggregation-induced emission. Dyes Pigments 2015; 119: 62-9.

[47] Yuan W Z, Tan Y Q, Gong Y Y, Lu P, Lam J W Y, Shen X Y, Feng C F, Sung H H, Lu Y W, Williams I D, Sun J Z, Zhang Y M, Tang B Z. Synergy between twisted conformation and effective intermolecular interactions: strategy for efficient mechanochromic luminogens with high contrast. Adv Mater 2013; 25: 2837-43.

Table 1 Optical properties of compounds **3a**–**3d** and emission wavelengths under various external stimuli

Compounds	λ_{abs}(nm)/ε (10^4 M^{-1} cm^{-1})[a]	Φ_F (%)[b]	$\lambda_{pristine}$(nm)[c]	$\lambda_{grinded}$(nm)[c]	λ_{fuming}(nm)[c]	$\Delta\lambda$(nm)[d]	λ_{em}[e]/λ_{em}[f](nm)
3a	301(2.47)/333(2.63)	38.1	448	469	449	21	475/481
3b	301(2.43)/333(2.60)	54.6	454	481	453	29	479/475
3c	299(2.62)/324(2.58)	60.4	440	463	442	23	473/468
3d	299(2.59)/324(2.59)	65.7	446	472	445	26	476/471

[a] Measured in pure THF; [b] Measured in crystalline solid; [c] Solid emission wavelength; [d] $\Delta\lambda=\lambda_{grinded}-\lambda_{pristine}$; [e] Measured in THF/water mixtures (f_w = 95%); [f] Measured in film.

Table 2 Electrochemical properties and thermostability of compounds **3a**–**3d**

Compounds	E^{ox}_{onset} (V)	HOMO (eV)		LUMO (eV)		E_g (eV)		T_g/T_d (°C)
		Exptl[a]	Calc	Exptl	Calc	Exptl[b]	Calc	
3a	1.16	-5.47	-5.28	-2.30	-1.47	3.17	3.81	87.6/348
3b	1.11	-5.42	-5.27	-2.25	-1.46	3.17	3.81	91.1/351
3c	1.12	-5.43	-5.32	-2.21	-1.42	3.22	3.90	53.8/319
3d	1.13	-5.44	-5.35	-2.22	-1.45	3.22	3.90	40.5/340

[a] HOMO levels were calculated using the following equations: HOMO = –e(E_{onset}–0.49 V) –4.8 eV, where the value 0.49 V is for FOC versus SCE electrode. [b] Estimated from the onset of the absorption spectra: 1240/λ_{onest}.

Table 3 Electroluminescence properties of the OLED devices

Device	V_{on}(V)[a]	EL (nm)[b]	FWHM[c]	L_{max} (cd/m^2)[d]	η_C (cd/A)[e]	η_P (lm/w)[f]	CIE (x,y)
I (3b)	3.3	436	85	2470	1.48	1.05	(0.180,0.171)
II (3c)	4.8	432	66	843	2.28	1.12	(0.179,0.149)

[a] Turn-on voltage (V) at a luminance of 1 cd/m^2; [b] Peak wavelength EL spectra; [c] Full-width at half maximum; [d] Maximum luminance (cd/m^2); [e] Maximum of luminance efficiency (cd/A); [f] Maximum power efficiency.

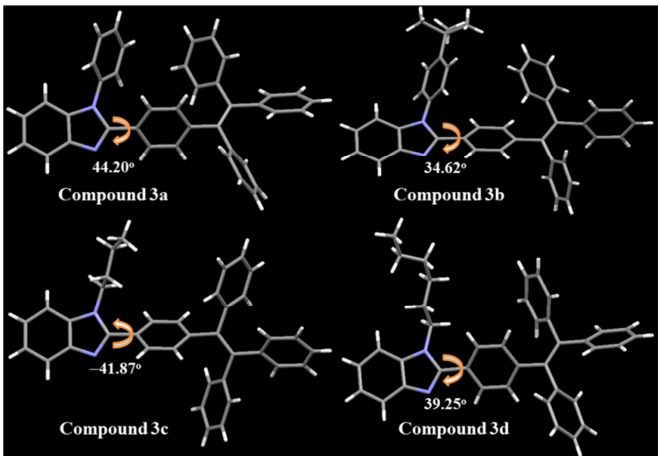

Fig. 1 Crystal structures of compounds **3a**–**3d**.

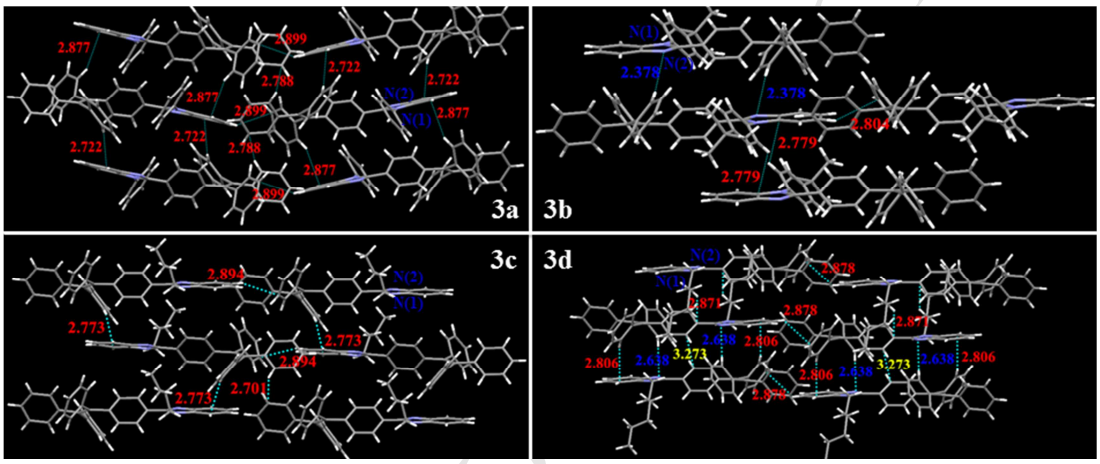

Fig. 2 The schematic intermolecular interactions in the crystal of compounds **3a**–**3d**, the red, blue and yellow numbers represent C-H---π, C-H---N and π-π interactions, respectively.

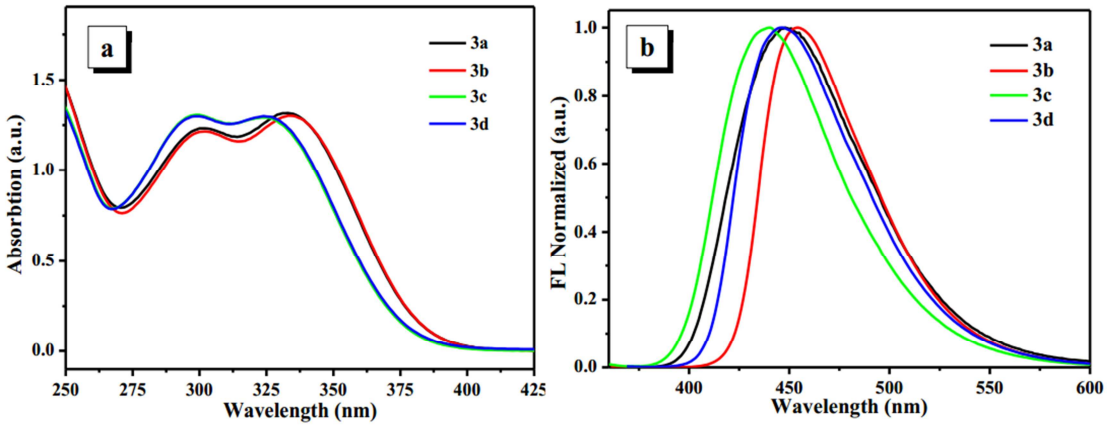

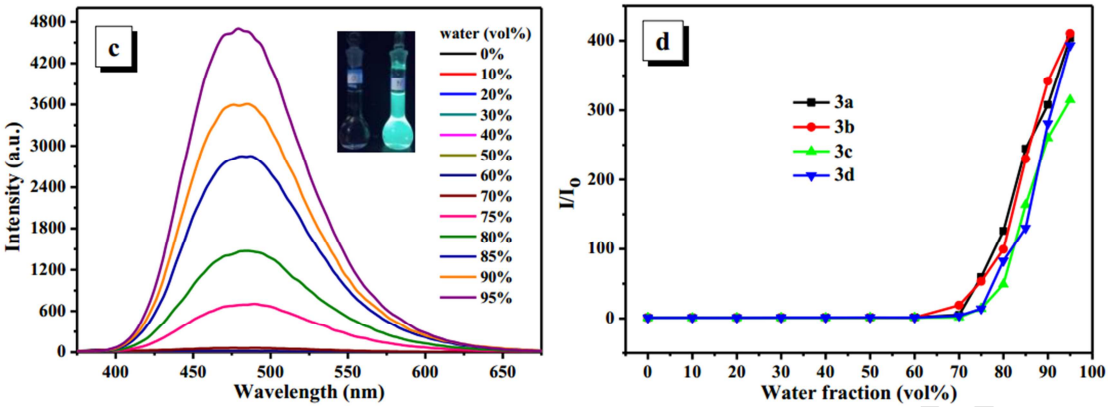

Fig. 3 (a) UV-visible spectra of the dilute solutions of compounds **3a**–**3d** in THF (concentration: 50 μM). (b) Normalized emission spectra of the compounds **3a–3d** recorded in pristine solid. (c) Fluorescence spectra of **3a** in THF-water mixtures with different f_w, inset photograph: compound **3a** in f_w =0 and 95% solvents under UV illumination. (d) Plots of (I/I_0) values versus THF/H_2O mixtures of compounds **3a**–**3d**, where I_0 is the PL intensity in pure THF solution. Concentration: 50 μM; EX wavelength: 350 nm; intensity calculated at λ_{max}.

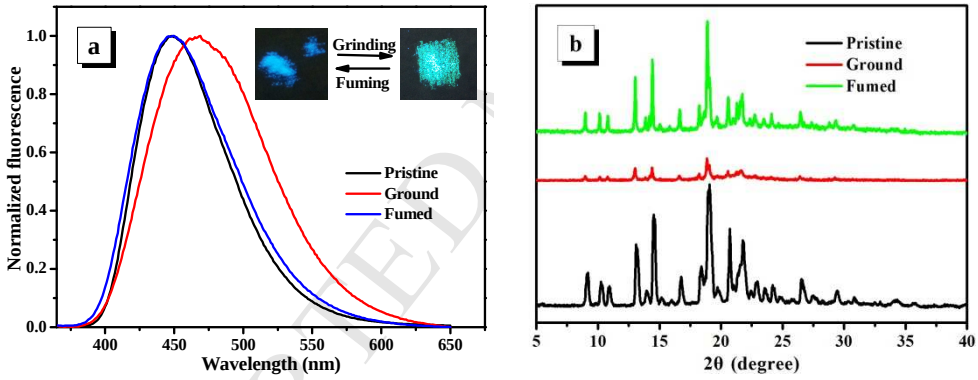

Fig. 4 (a) Emission spectra of **3a** as pristine, grinded and fumed solids, inset photographs: compound **3a** in pristine (left) and ground (right) forms under UV illumination. (b) Powder X-ray diffraction patterns of **3a** in pristine, ground and fumed forms.

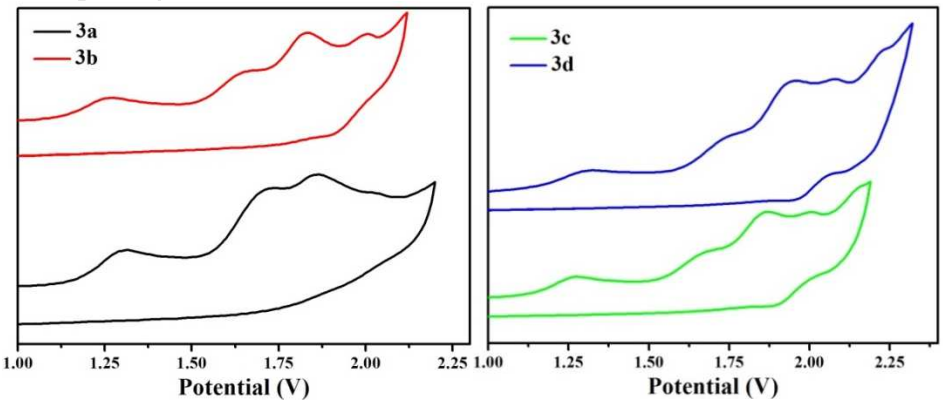

Fig. 5 Cyclic voltammograms of compounds **3a-3d**.

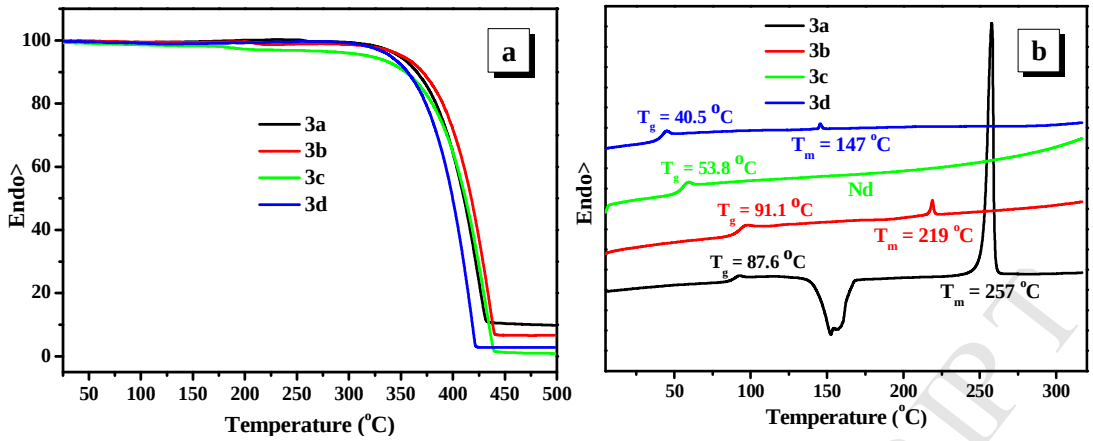

Fig. 6 (a) Thermogravimetric analysis (measured in crystal solid) and (b) DSC curves (second heating scan) of compounds **3a**–**3d** recorded under nitrogen at a heating rate of 10 °C min^{-1}.

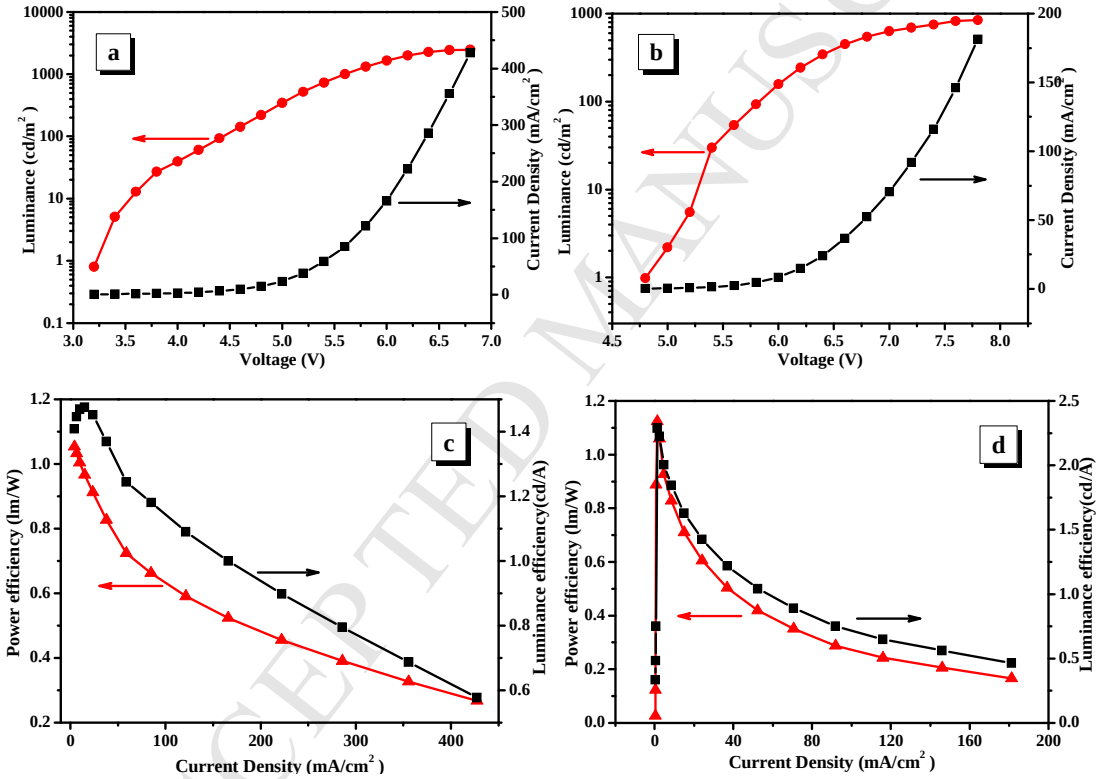

Fig. 7 The current density-voltage-luminance curves of the compounds **3b** (a) and **3c** (b); Luminance efficiency and Power efficiency of the compounds **3b** (c) and **3c** (d).

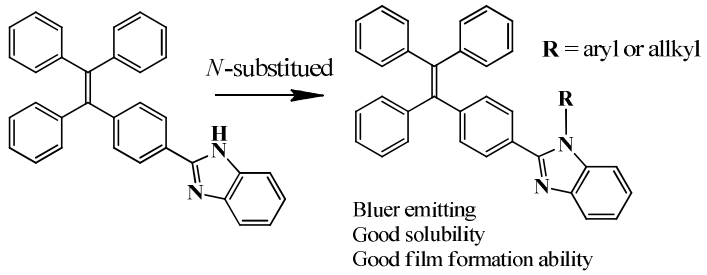

Scheme 1 Molecular modification strategy for tetraphenylethene-based benzimidazoles.

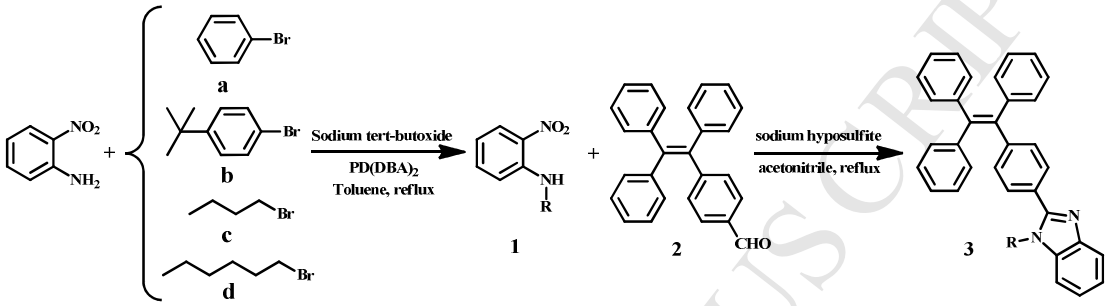

Scheme 2 Synthetic procedures for compounds **3a**–**3d**.

Highlights

- A new series of blue luminogens *N*-substituted tetraphenylethene-based benzimidazoles were synthesized.
- Crystal structures, photophysical properties and theoretical calculation of compounds **3a**-**3d** have been studied.
- Compounds **3a**-**3d** show fast-reversible mechanochromism under DCM vapor condition.
- Blue OLEDs employing compounds **3b** and **3c** as non-doped emitters were fabricated.